

## Influence of Inverter Switching Conditions on PMBLDC Motor Performance

Dr. Jamal Abdul-Kareem Mohammed

Electromechanical Engineering Department, University of Technology/Baghdad

Email:shwesh67@yahoo.com

Received on: 17/10/ 2011 & Accepted on: 7/6/ 2012

### ABSTRACT

Permanent Magnet Brushless DC (PMBLDC) motors are generally powered by a conventional three-phase voltage source inverter (VSI) or current source inverter (CSI) which is controlled using rotor position. By varying the commutation (switching) angles of the transistors in the inverter circuit, the performance of these motors could be greatly varied. This can be studied in this paper using the dynamic motor model, which was performed using Matlab/Simulink software package. A study on the influence of switching angles on motor performance shows that the motor operates better when advancing the switching angle, and there is a certain angle at which the motor operates with the highest efficiency. An improvement of the different operating characteristics of PMBLDC motor has been accomplished by adjusting the chosen set of the switching angles and using appropriate conduction angles.

**Keywords:** Switching angle, PMBLDC motor, Performance

### تأثير شروط التشغيل لعاكس الفولتية على أداء محرك التيار المستمر ذو المغناطيس الدائم والخالي من الفرش الكربونية

#### الخلاصة

تغذى محركات التيار المستمر ذو المغناطيس الدائم والخالية من الفرش الكربونية بشكل عام من العاكس التقليدي للفولتية أو التيار ثلاثي الأطوار، حيث تتم السيطرة على المحرك عن طريق تحديد موقع الجزء الدوار. بتغيير زوايا تشغيل الترانزستورات الخاصة بدائرة العاكس يمكن تغيير أداء تلك المحركات بشكل كبير. حيث تتم دراسة ذلك الأداء في البحث الحالي باستخدام الموديل الديناميكي للمحرك وبتوظيف برنامج المحاكاة (Matlab/Simulink). لقد بينت الدراسة الخاصة بتأثير زوايا التشغيل على أداء المحرك بأن المحرك الحالي يعمل بشكل أفضل عند تقديم زوايا التشغيل، حيث إن هناك زاوية تشغيل معينة تجعل المحرك يعمل بأقصى كفاءة. وعليه يمكن تحسين الخصائص التشغيلية المتنوعة للمحرك بتنظيم مجموعة من زوايا التشغيل واختيار الزوايا الأمثل منها.

### INTRODUCTION

Conventional DC motors are highly efficient, however, they need a commutator and brushes which are subject to wear and require maintenance. This deficiency can be overcome by the new type of DC drive based on brushless DC motors. The brushless DC motors are distinguished not only by the high efficiency but also by their low maintenance. The brushless DC

motors are permanent magnet motors where the functions of commutator and brushes were implemented by solid state switches [1].

Brushless DC motors find use in many applications ranging from printer head motors to large conveyor belt drivers. An example where constant torque control is used is in grinding mills, while constant speed operation is typically used for conveyor belt drives in process control plants. On the other hand, a wide range of constant power operation is highly desirable for Electric Vehicle (EV) applications because it can minimize the required motor size, and can also facilitate high speed cruising [2].

The PMSM motor consists of a wound stator and a rotor. The rotor just has permanent magnets and rotates synchronously with the magnetic field generated by the stator winding. At the motor start-up, the rotor has zero speed. Due to its high inertia, it cannot instantaneously shoot to its synchronous speed. However, this can happen if the stator winding is supplied with frequency, rising gradually from 0 to its rated value. To do this, the motor has to be supplied from a variable frequency inverter as shown in Fig. 1. In this paper three-phase inverter is considered. The frequency can be controlled when the motor itself can set an appropriate frequency value required for its actual speed. In this case, the motor must be equipped with a speed or position sensor [3].

The commutation instances of the PMSM motor from the current and voltage signals which are accomplished by the electronic switches, supplies current to the motor windings in synchronization with the rotor position [4]. Therefore, one of the main factors which influence the performance of the motor is the commutation (switching) angle of the inverter transistors. As the switching angle is advanced, the difference between the back-*emf* induced in the phase winding and supply phase voltage increases, and the torque thereby increases. However, there exists an optimal advanced angle, beyond which the drive performance deteriorates.

C-L Chiu, et.al [5] had used the finite-element method to simulate the optimal shift angle to improve efficiency and torque performance of a single-phase BLDC motor. B-G Gu, et.al [6], had been presented the lead angle adjustment scheme based on the mathematical method to get low copper loss and high efficiency induced by the low motor currents. S.M. Sue, et.al [7] had presented a phase advanced commutation scheme for IPM-BLDC motor drives. The proposed scheme can achieve higher efficiency and more extended speed range than the conventional control scheme does. M. A. Enany, et.al [8], proposed the method to simply reduce the torque ripples and improve motor operation by varying the switching-on and the switching-off angles for motor phase current and for same speed.

The current paper, aims by using Matlab/Simulink to study the influence of inverter switching conditions on motor performance, as well as investigating the effects of advancing the switching angles on improving of motor operation characteristics and reducing the torque ripple.

### INFLUENCE OF SWITCHING ANGLE ON MOTOR PERFORMANCE

The winding inductance causes significant phase delay (lagging) on motor phase current waveforms. The results in the currents and the *emfs* waveforms being out of phase, and a negative torque component is generated, with a consequent

reduction of the overall torque. In order to get motor better performance, the phases are switched earlier to compensate the difference of the lagging angle as shown in Figure(2).

The performance of the motor depends on the maximum torque output, minimum torque ripple with a minimal current input.

The pulsating torque of the motor is the sum of the cogging torque and the ripple torque, torque generated by the interaction of the stator current magnetomotive forces ( $mmf_s$ ) and rotor electromagnetic properties, and it is desired to counteract the pulsating torque [9].

Normally, the supply phase voltage  $v_{sa}$  is in phase with electromotive force  $e_a$  induced in the phase winding. The switching angle  $\alpha$  between  $v_{sa}$  and  $e_a$  may be changed to improve the performance of the motor and there is an optimum value of switching angle to get the improved motor operation. In BLDC motors, the switching angle may vary accordingly to the controller of the inverter that is used as shown in Fig. 1 [1].

The motor has to be equipped with a position sensor placed between the coils in the intervals of  $180^\circ$  which informs the controller the position of the rotor magnetic pole, with respect to the particular stator phase winding and triggers the transistors. This is done in order to switch the motor on and off [4].

In the dynamic simulation, it is easy to switch the inverter voltage  $v_{sa}$  than  $i_a$ . The switching angle  $\alpha$  is referred to the  $emf$  waveform where  $e_a$  is equal to 0 as shown in Fig. 2.

Different arrangements of switching angles will lead to have wide variety of motor operation characteristics which increase the motor capabilities and extending the field for their practical applications.

**ANALYSIS OF MOTOR DYNAMICS**

To analyze the motor dynamics theoretically, the mathematical model of the motor is developed.

The simulation of the motor drive is done using Matlab/ Simulink software package.

**Mathematical Model of the Supply-Inverter-Motor System**

The equivalent circuit of a brushless dc motor is shown in Fig 3.

It is assumed that the motor is connected to the output of the inverter, while the inverter input terminals are connected to a constant supply voltage.

The following assumptions are made:

1. All the elements are linear and no core losses are considered.
2.  $Emf_s$  and cogging torque vary sinusoidally with rotational angle  $\phi_e$
3. The three-phase motor windings are connected in star.
4. Due to surface mounted permanent magnets, windings inductance is constant.
5. Voltage drops across diodes, transistors and connecting wire inductances are ignored.

The voltage equations that govern this model are as follows [1,3].

$$\begin{aligned}
 v_A &= v_N + v_{sA} \\
 v_B &= v_N + v_{sB} \\
 v_C &= v_N + v_{sC}
 \end{aligned}
 \dots\dots (1)$$

, where  $v_{sA}$ ,  $v_{sB}$ ,  $v_{sC}$  are the inverter output voltages that supply the three-phase windings.  $v_A$ ,  $v_B$ ,  $v_C$  are the voltages across the motor armature windings.  $V_N$  is voltage at the neutral point as shown in Fig. 4.

Assuming symmetrical windings and balanced system, the voltage equation across the motor windings can be written as follows:

$$\begin{bmatrix} v_A \\ v_B \\ v_C \end{bmatrix} = \begin{bmatrix} R_A & 0 & 0 \\ 0 & R_B & 0 \\ 0 & 0 & R_C \end{bmatrix} \begin{bmatrix} i_A \\ i_B \\ i_C \end{bmatrix} + \frac{d}{dt} \begin{bmatrix} L_S & 0 & 0 \\ 0 & L_S & 0 \\ 0 & 0 & L_S \end{bmatrix} \begin{bmatrix} i_A \\ i_B \\ i_C \end{bmatrix} + \begin{bmatrix} e_A \\ e_B \\ e_C \end{bmatrix} \quad \dots\dots (2)$$

, where  $i_A$ ,  $i_B$ ,  $i_C$  are the motor phase currents.  $L_S=L-M$ , where the self  $L$  and mutual  $M$  inductances are constant for surface mounted permanent magnets on the cylindrical rotor and the windings are symmetrical. Therefore, the phase self inductances;  $L_A=L_B=L_C=L$  and mutual inductances;  $M_{AB}=M_{BC}=M_{CA}=M$ , as well as, the phase winding resistances are equal too;  $R_A=R_B=R_C=R_A$ . Therefore Eq. 2 can be rewritten as:

$$V_A = R_A I_A + \frac{d}{dt} L_A \cdot I_A + E_A \quad \dots\dots (3)$$

The electromotive force induced in the phase A winding shown in Fig.5 is

$$e_a = K_E w_m \sin(j_e) \quad \dots\dots (4)$$

, where:

$K_E$  – Back-emf Constant (V.s/rad)

$\omega_m$  - Rotor angular speed;

$$w_m = \frac{1}{p} \frac{dj_e}{dt} \quad \dots\dots (5)$$

$\phi_e$  - Rotor position

$p$  - Number of pole pairs.

Choosing phase-A as the reference, the matrix form of electromotive force, can be written as follows:

$$E_A = \frac{K_E}{p} \begin{bmatrix} \sin j_e \\ \sin(j_e - 2p/3) \\ \sin(j_e - 4p/3) \end{bmatrix} \frac{dj_e}{dt} \quad \dots\dots (6)$$

, where  $\phi_e$  is the angle between a particular phase A and the rotor at any given time. Now, with assuming the inverter input power  $P_{in}$  = inverter output power  $P_{out}$  in Fig. 3, the inverter input current can be written as:

$$i_s = \frac{1}{V_s} (i_A n_{sA} + i_B n_{sB} + i_C n_{sC}) \quad \dots\dots (7)$$

, where  $V_s$  is the supply voltage.

The mechanical system of the motor can be defined by the following equation:

$$T_{em} = T_J + T_B + T_s + T_{cog} + T_L \quad \dots\dots (8)$$

The torque components of Eq. 8 are expressed by the following equations:

- Inertia torque:

$$T_J = J_{eq} \frac{d\omega_m}{dt} \quad \dots\dots (9)$$

- Viscous friction torque:

$$T_B = B.\omega_m \quad \dots\dots (10)$$

- Coulomb friction torque:

$$T_s = sign(\omega_m)T_d \quad \dots\dots (11)$$

- Cogging torque:

$$T_{cog} = T_{mc} \sin(2j_e + \alpha) \quad \dots\dots (12)$$

-  $T_L$  and  $T_{em}$  are load and electromagnetic torque, respectively.

Other symbols used in above equations are:

$J_{eq} = J_M + J_L$  is the equivalent moment of inertia (moment of inertia of motor and load, respectively).

$B$ -Friction coefficient

$T_{mc}$  - Cogging torque amplitude

$T_d$  - Amplitude of  $T_s$

$\alpha$  - Displacement angle of cogging torque = switching angle  $\alpha$ .

- The electromagnetic torque for three phase motor is dependent on the phase current  $i$ , speed  $\omega_m$  and electromotive force  $e$  and can be represented as:

$$T_{em} = \frac{e_A i_A}{\omega_m} + \frac{e_B i_B}{\omega_m} + \frac{e_C i_C}{\omega_m} = K_E (f_a(j_e) i_A + f_b(j_e) i_B + f_c(j_e) i_C) \quad \dots\dots (13)$$

, where:  $f_a(j_e) = \sin j_e$ ,  $f_b(j_e) = \sin(j_e - 2p/3)$  and  $f_c(j_e) = \sin(j_e - 4p/3)$ .

**RESULTS AND DISCUSSION**

The simulation of the PMBLDC motor was done using the software package Matlab/Simulink. For this purpose, the motor’s block diagram was constructed using the mathematical model of the motor, as shown in Fig. 6. In this diagram, the electromotive forces  $e_A$ ,  $e_B$  and  $e_C$  of the motor are generated by rotor position signal  $\varphi_e$  and appropriate functions:  $f_a(\varphi_e)$ ,  $f_b(\varphi_e)$ , and  $f_c(\varphi_e)$ . The phase voltages  $v_{sA}$ ,  $v_{sB}$  and  $v_{sC}$  in the motor Block are generated by position signal  $\varphi_e$ .

The speed, torque, current, input and output power waveforms shown in Fig. 7, were recorded and analyzed. Fig. 7.a shows the start-up process of the motor at zero switching angle ( $\alpha=0^0$ ). The figure depicts the waveforms of source current  $i_s$ , phase voltage  $v_{sa}$  and phase current  $i_a$ , electromagnetic torque  $T_{em}$ , and speed  $\omega_m$  in dynamic condition.

The inverter was supplied with a voltage of 42V DC and the motor loaded with a rated torque of 0.56 N.m. All the motor parameters are listed in Table 1. The phase

voltages  $v_{sA}$ ,  $v_{sB}$ , and  $v_{sC}$  are quasi-square waves of 21V DC. However, notice how the phase current  $i_a$  is distorted from the quasi-square wave shape. This is due to the inductance effect.

After the initial start-up, the torque  $T_{em}$  oscillates around some very low value and the speed oscillates around 311.5 rad/sec (no-load speed).

After the start-up process, the motor reaches steady-state at around 0.02 sec and a load torque with 0.56 N·m is applied at this time. The torque  $T_{em}$  rises steeply as the motor start to run.

The motor speed will decrease and oscillate after loading with the rated load around steady-state speed value of 248 rad/sec. The electromagnetic torque  $T_{em}$  depends on phase currents, motor constant  $K_m$ , speed and electromotive force and equal to 0.6921 N.m (recalling Eq. (13) oscillates around very low value) as listed in Table(3).

Table (2) lists the motor specifications and Fig(7.b) represents the steady-state characteristics of the motor with load.

The motor efficiency can be calculated as follows:

$$h = (P_{out} / P_{in}) \times 100 \quad \dots\dots (14)$$

where the output (load) power on the motor shaft,

$$P_{out} = T_L \cdot \omega_m \quad \dots\dots (15)$$

and the input power of the inverter equal to the input power of the motor,

$$P_{in} = V_s \cdot I_s \quad \dots\dots (16)$$

where,  $V_s$  is the source voltage and  $I_s$  is the average value of source current.

The quantities  $P_{in}$ ,  $P_{out}$ , and  $\eta$  were calculated as average values while the motor currents as *rms* values.

From the speed and torque waveform plots shown in Fig 7, severe distortions in the waveforms of speed and torque were observed, which was due to the electronic commutation (switching of the transistors) as well as the presence of cogging torque.

The same running of simulation is carrying out to obtain waveforms shown in Figure(8), by introducing an optimum value of switching angle ( $\alpha = -5.95^\circ$ ) at rated load to get maximum efficiency  $\eta_{max}$ . It can show from the figure that the amplitude of the distortion in current decreases with respect to that in Fig. 7 when there is no switching introducing. Therefore, the ripple in torque and thus speed will decrease too.

The spectrum analysis of the motor torque in Figure(9) shows, how the motor by introducing an optimum switching angle ( $\alpha = -5.95^\circ$ ) exhibits less average torque by amount of 2.66% and less distortion in torque *THD* by 45.42% than that when there is no switching action.

From Figs(7) and (8), Table (3) one can notice that the percentage differences in the motor performance with and without getting advanced switching angle for the inverter transistors. It can be shown from the table that the proposed motor at rated load operates better by introducing a commutation angle advance  $\alpha = -5.95^\circ$ .

In brushless dc machines, it is very difficult to get low cogging torque and low ripple torque simultaneously. Sometimes reducing the cogging torque leads to reduction of the average torque  $T_{em}$  as shown Table (3).

To examine the influence of changing the switching angle on motor performance, the simulation was carried out for the switching angles  $\alpha$  in the range of ( $0^\circ$  to  $-25^\circ$ ).

The simulation results were plotted in the form of performance characteristics of average values of source current  $I_s$ , input power  $P_{in}$ , output power  $P_{out}$ , torque  $T_{em}$ , speed  $\omega_m$  and efficiency  $\eta$  as shown in the 3-D plots of Fig(10 (a-f)).

The plots represent the motor performance determined with loading from no-load until four times the rated load ( $\sim 2.2$  N.m) with varying in the switching angle of the transistors from ( $0^\circ$  until  $-25^\circ$ ). It can be concluded from the  $\eta$  curve that the optimum values of  $\alpha$  increases with load. The negative sign of the angle means that the transistors are switched earlier with respect to the induced EMF waveforms.

From the previous results, the variation of the optimum switching angles advance to get  $\eta_{max}$  with loading and then improving the motor operation and the corresponding maximum motor efficiencies can be deduced as shown in Fig(11).

The motor efficiency has maximum rated value (89.73%) when the switching angle is  $\alpha = -5.95^\circ$  while it is equal to (93.03%) at  $\alpha = -18^\circ$  at 1.7N.m load ( $\sim 3$  time the rated load).

The plots in Fig(12) represent the electromechanical characteristics of the motor in the steady-state obtained in simulation using dynamic model of the motor. These curves chosen for three different cases of switching angles *i*) for the optimum values of switching angles (to get  $\eta_{max}$  at each value of load), *ii*) without switching angle ( $\alpha = 0^\circ$ ), and *iii*) with switching angle ( $\alpha = -5.95^\circ$  to get  $\eta_{max}$  at rated load). From the plots, it can be noticed that, the motor pulls less source current and input power in the first case (optimum  $\alpha$ 's) and has approximately higher output power, speed and efficiency than the other two cases. Also, it can be seen that for the optimum case, the motor speed is approximately stable for the whole range of  $T_L$  around some value, while it decreases with loading in the other two cases. Also, the efficiency  $\eta$  values are stable around some value after certain load (about 1 N.m) for the first case, while it decreases for that load in other cases.

In general, the motor operates better when advancing the switching angle, where the motor operates with the highest efficiency.

For increasing the motor capabilities and extending for their practical applications, different electromechanical characteristics for constant speed, constant power, and constant load operation of the motor under various switching angle advance conditions are displayed respectively as in Figs. (13-15).

The curves (a) in the Figs. 13 and 14, respectively, represent the selected angles  $\alpha$  to get constant speed and constant power operation with loading, while the curves (b and c) in the figures above acts the electromechanical characteristics at constant speed and power, respectively. It can see that for constant speed, the power is in direct linear proportion with load, while for constant power, the speed has an inverse proportion with load. Also it can see from Fig. 13 (b and c) that the loading range is wide at no-load speed and decreases with varying speed below or over the no-load value.

Curves (a and b) in Figure (15). show the motor speed and power with selected angles  $\alpha$  for constant torque load operation while curves (c and d) act the

corresponding electromechanical characteristics. It can be noted that speed range is wide at lower loads and decreases with loading while power range is approximately constant.

### CONCLUSIONS

Based on the simulation results, by varying the commutation angle of the transistors in the inverter circuit, the performance of the motor could be greatly varied. Advancing of switching angles had been proposed to improve the motor performance.

From simulation results, the differences between operation with and without switching angles advance are noticed, and it can be easily deduced that increasing the advance switching angle leads to lower phase current, lower torque ripples, higher no load speed and higher efficiency comparing with normal operation.

The motor, from the simulation of the model, attains maximum efficiency at switching angle  $\alpha = -5.95^\circ$  at rated load increased by around 30% of that with zero switching angle  $\alpha = 0^\circ$ . The distortion *THD* in torque at this value of angle decreases at rated load with respect to  $\alpha = 0^\circ$  about 45.42%. Decreasing in torque distortion causes fewer ripples in the speed waveform.

As the load torque is increased from no load, it is desirable to change the optimum value of  $\alpha$  for each value of  $T_L$  to get maximum performance for driving any load and give improved operation.

The results of analysis have clearly shown that the different electromechanical operation characteristics of the brushless DC motor can be improved considerably simply by adjusting the chosen setting of the phase-advance angle and using appropriate conduction angles.

### REFERENCES

- [1]. Sunil K. Challa, Comparative Study of Axial Flux Permanent Magnet Brushless DC Motor Operating with the Winding connected in Single-phase and Two-phase System, MSc. Louisiana State University, August, 2006.
- [2]. Varsani, A. Low Cost Brushless DC Motor Controller, BSc. Thesis, University of Queensland, Nov., 2003.
- [3]. Pratapa, R. K. Modeling and Analysis of Radial Flux Toroidally Wound Twin Rotor Permanent Magnet Motor, MSc. Thesis, Louisiana State University, 2010.
- [4]. Singh and S. Singh, B. "State of the Art on Permanent Magnet Brushless DC Motor Drives", Journal of Power Electronics, Vol. 9, No. 1, January 2009, pp.1-17.
- [5]. C-L Chiu, Y-T Chen, Y-L Liang, and R-H Liang, Optimal Driving Efficiency Design for the Single-Phase Brushless DC Fan Motor IEEE Transactions on Magnetics, Vol. 46, No. 4, April 2010, pp. 1123-1130.
- [6]. B-G Gu, J-S Park, J-H Choi, S-h Rhyu, and I-S Jung, Optimal Lead Angle Calculation for Brushless DC Motor, The 2010 International Power Electronics Conf., pp. 1416-1420.
- [7]. Sue, S.M. K.L. Wu, J.S. Syu, and K.C. Lee, "A phase advanced commutation scheme for IPM-BLDC motor drives," ICIEA 2009.
- [8]. Mohamed. A. Enany, Hamed. M. Elshewy, Fathy E. Abdel-kader," Brushless DC Motor Performance Improvement through Switch-on and Switch-off Angles

Control", Proceedings of the 14<sup>th</sup> International Middle East Power Systems Conf., Cairo University, Egypt, Dec. 19-21, 2010, Paper ID 285, pp. 786-790.  
 [9]. De Four, R. E. Ramoutar, J. Romeo and B. Copeland, Pulsating Torque in Brushless DC Motors, Report, Indies, 2007.

**Table (1): Electrical and parameters of the motor.**

Per phase resistance, $R_A$	0.077 $\Omega$
Supply Voltage, $V_s$	42V
Per phase Inductance, $L_A$	0.21mH
Moment of Inertia, $J_{eq}$	$7.895e^{-7}$ Kg.m <sup>2</sup>
Back-emf Constant, $K_E$	0.073 V.s/rad
Rated Load Torque, $T_L$	0.56 N.m

**Table (2): Electromech. specifications of BLDC motor in steady-state.**

Supply Voltage, $V_s$	42V
Output Power, $P_{out}$	140.6 W
Input Power, $P_{in}$	202.9 W
Load Torque, $T_L$	0.56 N.m
Efficiency, $\eta$	69.3 %
Electromagnetic Torque, $T_{em}$	0.69 N.m
Speed, $\omega_m$	248 rad/sec
Phase Current, $I_a$	10.72 A

**Table (3): Motor performance with and without switching action at rated load.**

A (°)	$I_s$ (A)	$P_{in}$ (W)	$P_{out}$ (W)	$T_{em}$ (N.m)	$\omega_m$ (rad/sec)	$\eta$ (%)	Torque Distortion THD (%)	Torque Ripple (p-p) N.m	Speed Ripple (p-p) rad/sec
0	4.8305	202.883	140.602	0.6921	247.935	69.302	55.57	0.438	13
-5.95	4.2239	177.403	159.183	0.6737	281.07	89.73	30.33	0.315	8.5
Change(%)	-12.56	-12.56	+13.22	-2.66	+13.364	+29.47	-45.42	-28.1	-34.62

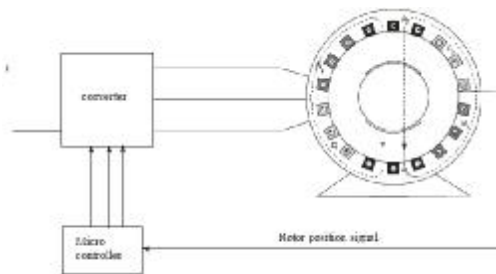


**Figure (1): Supply circuit scheme of PMSBLDC Motor.**

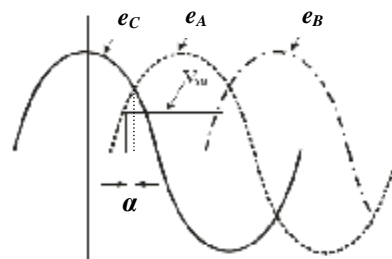


**Figure (2): Illustration of the switching angle  $\alpha$ .**

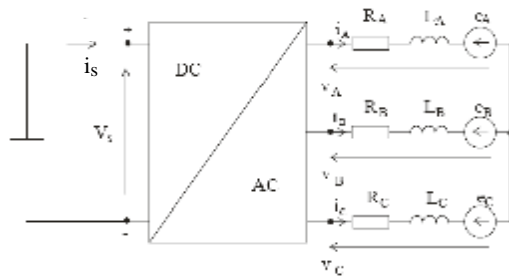
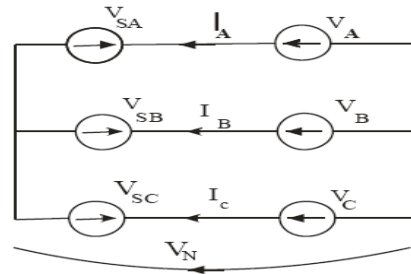


Figure (3): Equivalent circuit of the motor.



Figure(4): Schematic representing of Eq.1 .

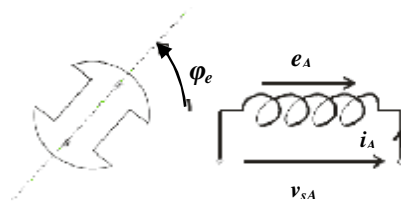
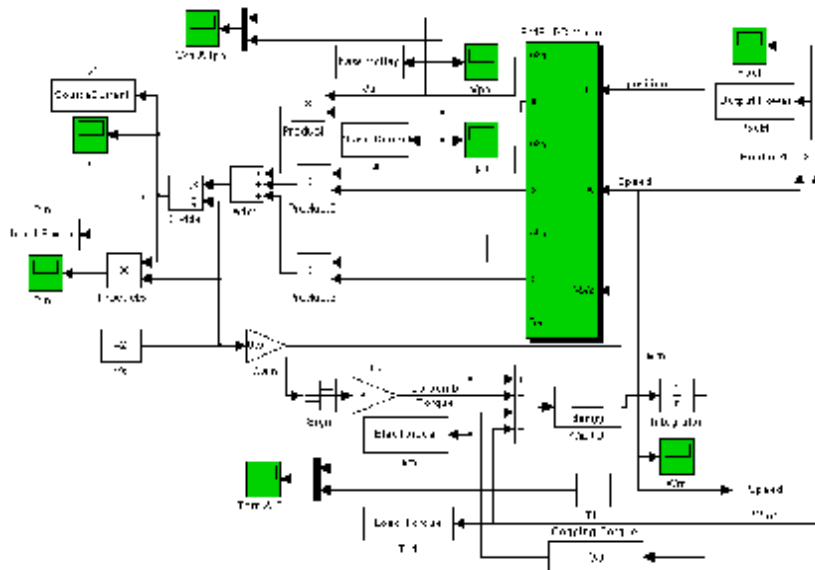


Figure (5): Position of the rotor with respect to the phase A.



Figure(6): Simulink block diagram of PMBLDC motor.

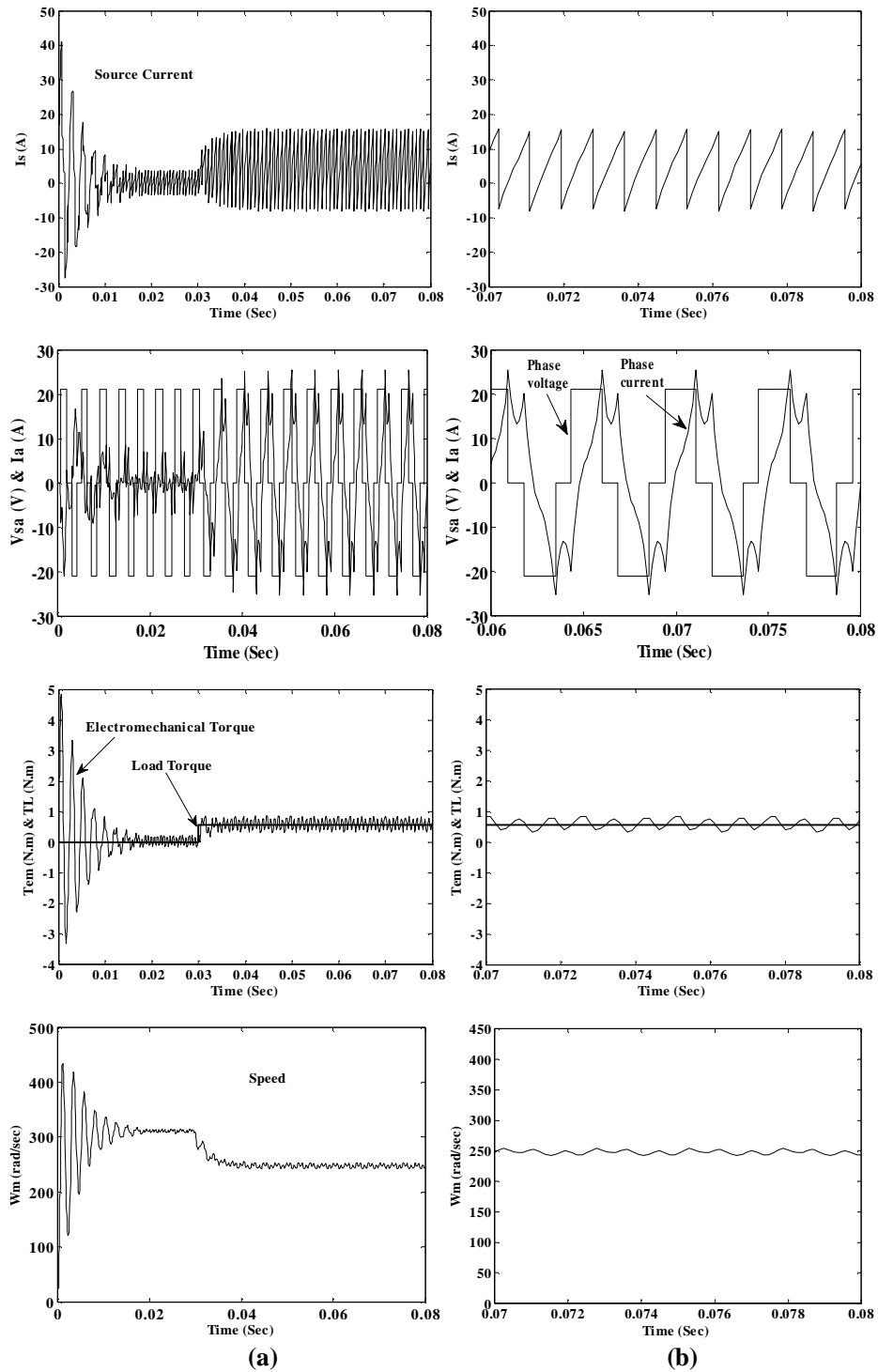


Figure (7): Waveforms of electromechanical quantities obtained from: (a) the start-up process of the BLDC motor, (b) steady-state [at zero switching angle].

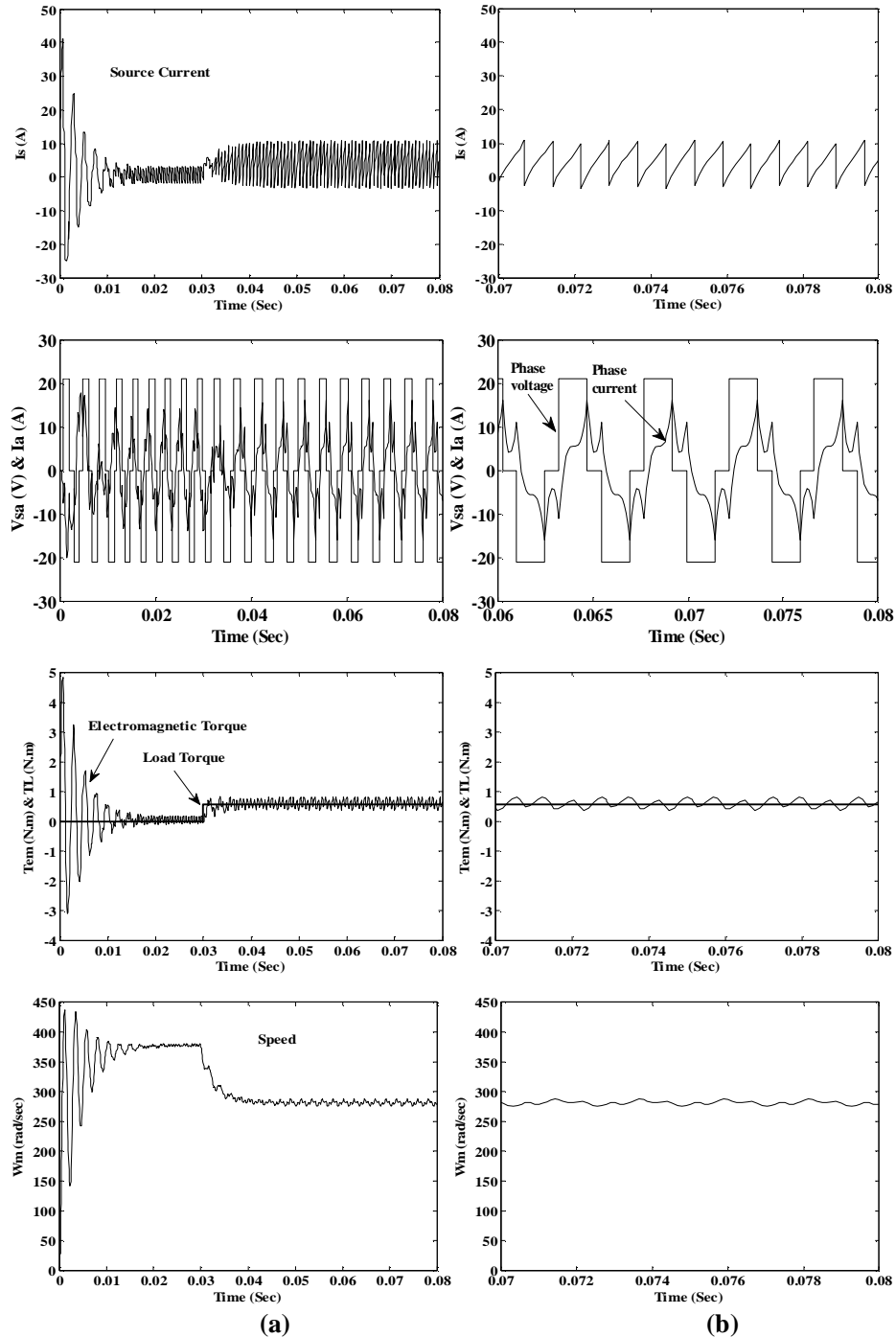
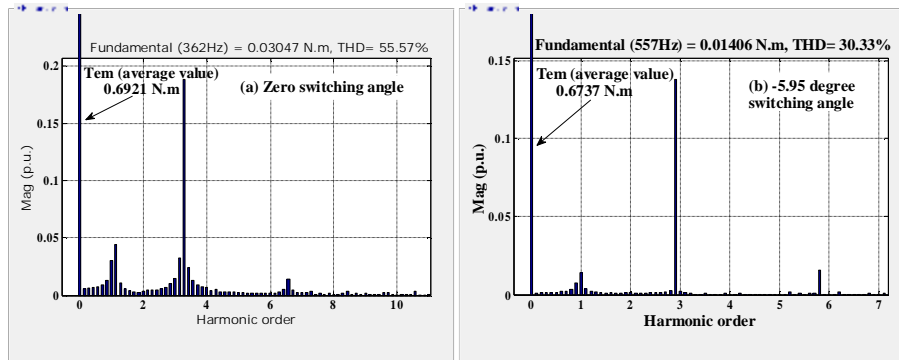


Figure (8): Waveforms of electromechanical quantities obtained from: (a) the start-up process of the BLDC motor (b) steady-state [at  $-5.95^\circ$  switching angle].



Figure(9): Harmonic Spectrum of motor torque with and without switching angle.

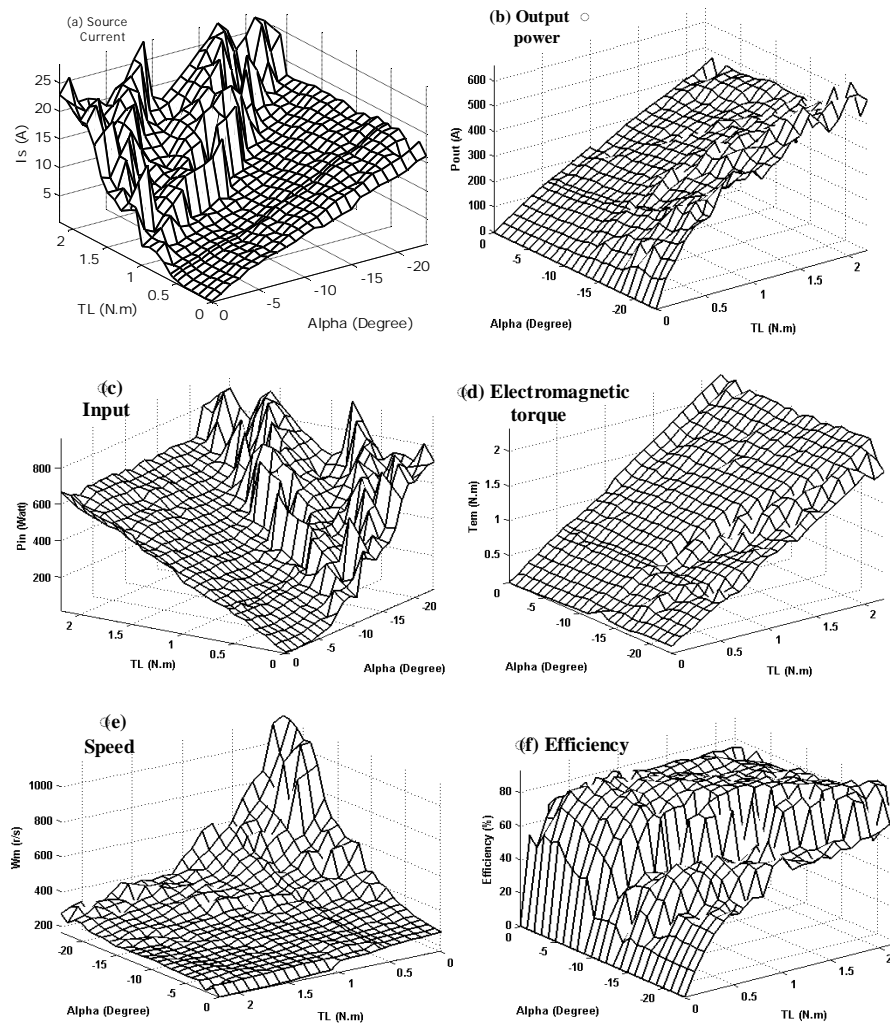


Figure (10): Motor performance versus switching angles  $\alpha$  with loading  $T_L$ .

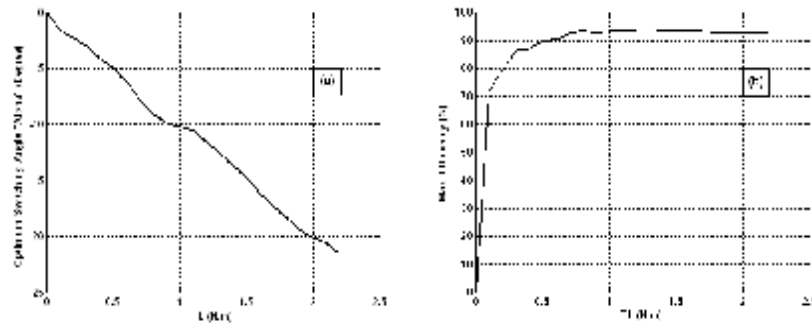


Figure (11): Optimum switching angles (a) and max. Efficiency (b) with loading.

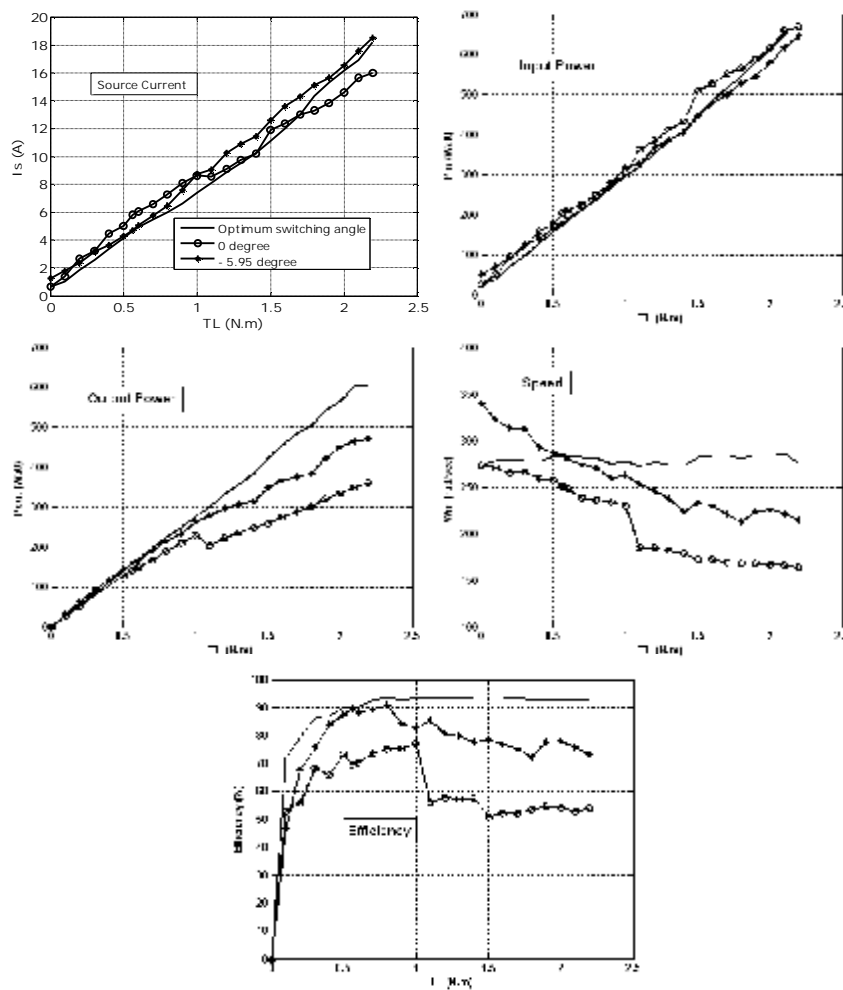


Figure (12): Electromechanical characteristics in steady-state with loading at different cases of switching angles ( $\alpha$  = Optimum switching angles, zero switching angle, and  $-5.95^\circ$  switching angle, respectively).

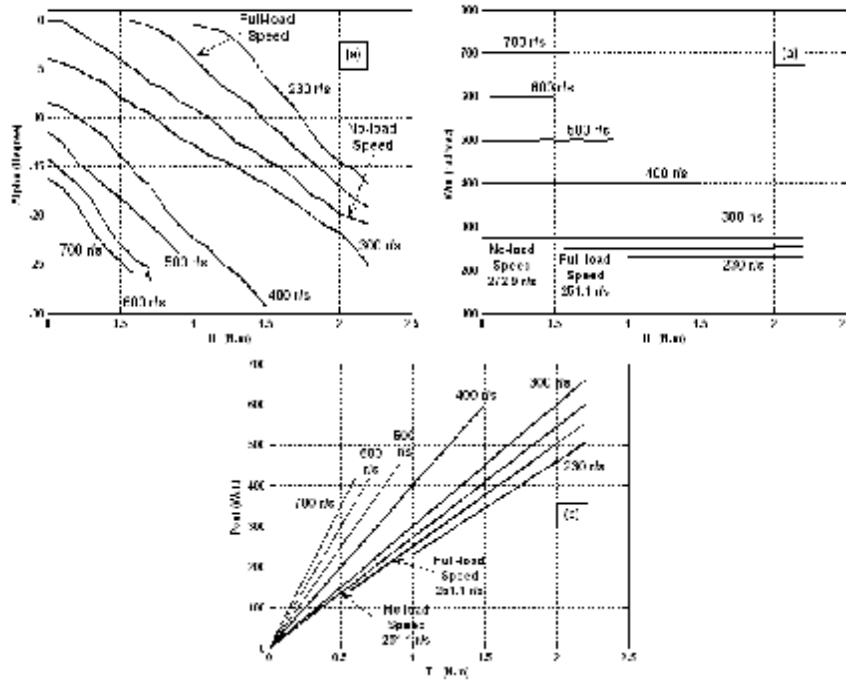
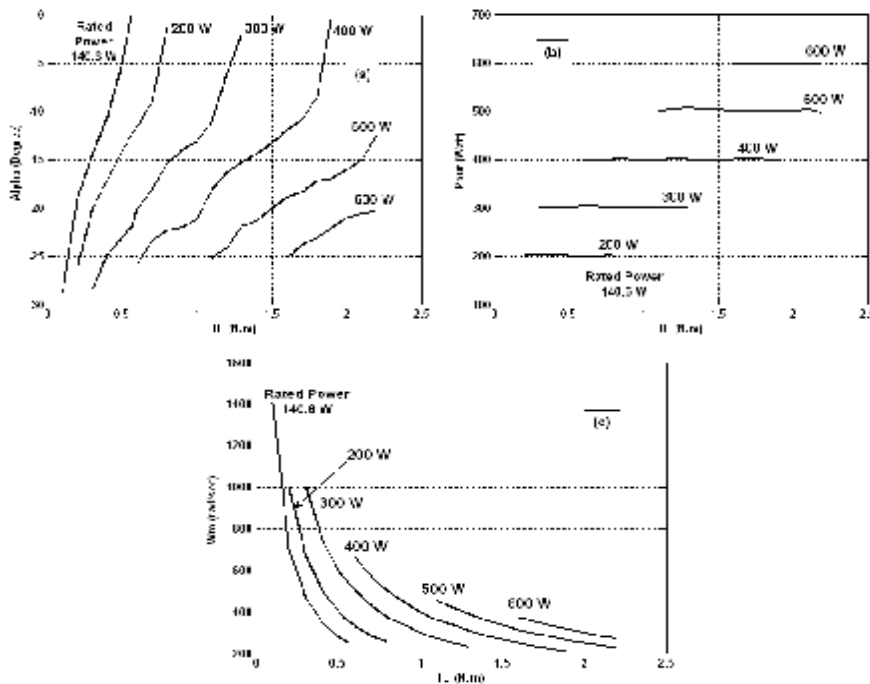


Figure (13): Switching angles  $\alpha$  with loading  $T_L$  for Constant Speeds (a) and the Corresponding Motor Characteristics (b&c).



Figure(14): Switching angles  $\alpha$  with loading  $T_L$  for Constant Power (a) and the Corresponding Motor Characteristics (b&c).

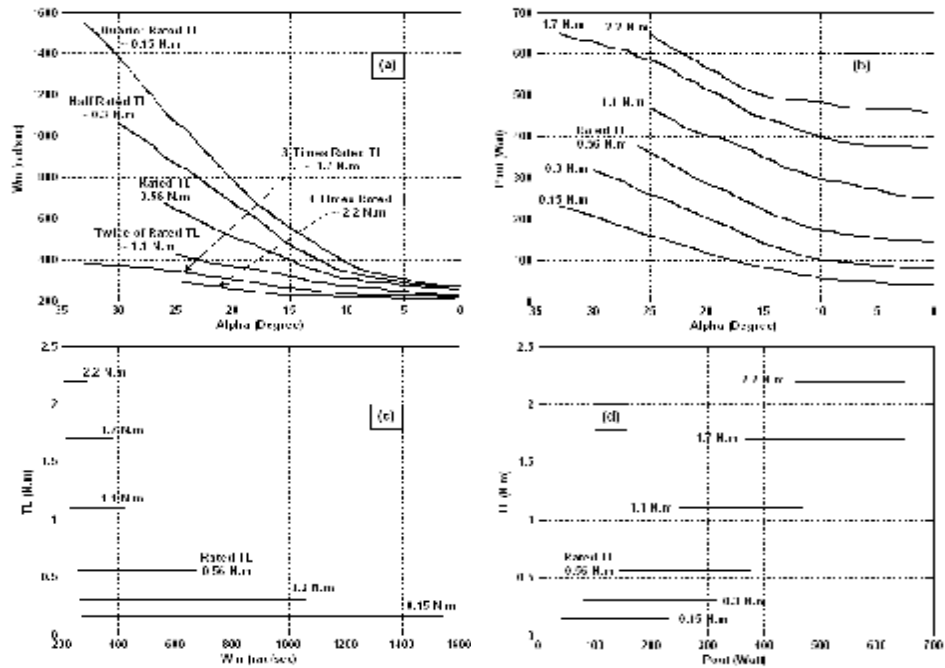


Figure (15): Motor Speed and Power vs. switching angles  $\alpha$  for Constant Torque Load (a&b) and the Corresponding Motor Characteristics (c&d).